OVERSTABILITY OF ACOUSTIC MODES AND THE SOLAR FIVE-MINUTE OSCILLATIONS

H. M. ANTIA, S. M. CHITRE, and D. NARASIMHA
Tata Institute of Fundamental Research, Homi Bhabha Road, Bombay 400 005, India

(Received 9 January; in revised form 12 May, 1981)

Abstract. The stability of linear convective and acoustic modes in solar envelope models is investigated by incorporating the thermal and mechanical effects of turbulence through the eddy transport coefficients. With a reasonable value of the turbulent Prandtl number it is possible to obtain the scales of motion corresponding to granulation, supergranulation and the five-minute oscillations. Several of the acoustic modes trapped in the solar convection zone are found to be overstable and the most unstable modes, spread over a region centred predominantly around a period of 300 s with a wide range of horizontal length scales, are in reasonable accord with the observed power-spectrum of the five-minute oscillations. It is demonstrated that these oscillations are driven by a simultaneous action of the κ-mechanism and the radiative and turbulent conduction mechanisms operating in the strongly superadiabatic region in the hydrogen ionization zone, the turbulent transport being the dominant process in overstabilizing the acoustic modes.

1. Introduction

A considerable amount of work has been done to study the solar velocity field which has two main components: convective motions manifesting as granulation and supergranulation (Beckers and Canfield, 1976), and oscillatory motions amongst which the five-minute oscillations (Leighton *et al.*, 1962) are most extensively documented (Frazier, 1968; Tanenbaum *et al.*, 1969; Deubner, 1972; Fossat *et al.*, 1974). The work of Deubner (1975) gave a detailed power-spectrum of the five-minute oscillations which opened up a new field of solar seismology to probe the solar convection zone. The later observation of the oscillatory power, with improved resolution, by Rhodes *et al.* (1977) and Deubner *et al.* (1979) established that the five-minute oscillations indeed represent nonradial acoustic modes in the solar atmosphere.

A number of proposals had been advanced to account for the five-minute oscillations and these are reviewed by Stein and Leibacher (1974). The currently accepted model based on the trapping of the acoustic waves in the subsurface layers of the Sun was proposed by Ulrich (1970) and Leibacher and Stein (1971). Ulrich (1970) attributed the overstability of the trapped p-modes to the radiative Cowling–Spiegel mechanism (Cowling, 1957; Spiegel, 1964) operating in the superadiabatic region below the photosphere. Ando and Osaki (1975) investigated the stability of nonradial oscillations for a solar envelope model with full effects of radiative dissipation included in the calculation, and found many overstable acoustic modes with their periods centred around 300 s and with a wide range of horizontal wavenumbers. Ando and Osaki claimed that the acoustic waves were overstabilized largely due to the κ-mechanism of the hydrogen ionization zone. However, the

Solar Physics **77** (1982) 303–327. 0038–0938/82/0772–0303 $03.75.

interaction between turbulent convection and oscillation was completely neglected in their work. Gabriel *et al.* (1975) took account of the thermal coupling between convection and non-radial oscillations to find an appreciable effect of the convective flux perturbation on the stability characteristics. The stochastic excitation of radial solar oscillations incorporating the effects of turbulent convection was discussed by Goldreich and Keeley (1977), but their results were rather sensitively dependent on the assumptions concerning the turbulent velocities and the spectrum of turbulent eddies. Berthomieu *et al.* (1979) considered the interaction between convection and oscillation to get all the p-modes of degree 200 and 600 to be stable. This calculation employs a generalized mixing-length formulation (Baker and Gough, 1979) based on the Boussinesq approximation to describe the turbulent fluctuations, and it is not clear how far the results are sensitive to this assumption since this will almost certainly affect the phase relationship between the radial velocity and the pressure fluctuation.

The stability of linear convective modes in the solar convection zone was investigated by Antia *et al.* (1981), (hereinafter referred to as Paper I) with the mechanical and thermal effects of turbulence included in an approximate manner through the eddy transport coefficients. For a reasonable choice of the turbulent Prandtl number the most unstable fundamental mode and the first harmonic were found to be in reasonable accord with the observed characteristics of granulation and supergranulation. Any reasonable theoretical ansatz should provide for the same choice of the turbulent Prandtl number, not only the most rapidly growing convective modes corresponding to granulation and supergranulation, but should also reproduce the acoustic modes closely resembling the observed features of the five-minute oscillations. We wish to investigate this problem in the present work by taking into account the interaction between convection and pulsation in an approximate manner through the turbulent heat conductivity and turbulent viscosity. We find that many of the acoustic modes trapped in the solar convection zone are overstable and the most rapidly growing modes occupy a region centred around a period of 300 s and spread over a wide range of horizontal scales from several thousand to a few tens of thousand kilometers. The essential conclusion of our work is that the simultaneous operation of the κ-mechanism and the turbulent conduction (convective Cowling) mechanism (Unno, 1976) is responsible for exciting the five-minute oscillations, the dominant contribution to the generation of self-excited acoustic waves arising from the convective Cowling mechanism.

2. Mathematical Formulation

A. GOVERNING EQUATIONS

The governing equations applicable to a viscous thermally conducting fluid layer are the usual hydrodynamical conservation equations for mass, momentum and energy. In the notation of Paper I these equations may be written in the following form:

Mass conservation:

$$\frac{\partial \rho}{\partial t}+\nabla \cdot (\rho \mathbf{v}) = 0;$$

momentum conservation:

$$\rho \frac{\partial \mathbf{v}}{\partial t}+\rho(\mathbf{v}\cdot\nabla)\mathbf{v} = \rho \mathbf{g}-\nabla P-\tfrac{2}{3}\mu\nabla(\nabla\cdot\mathbf{v})-$$

$$-\tfrac{2}{3}(\nabla\cdot\mathbf{v})\nabla\mu+\nabla\cdot[\mu(\nabla\mathbf{v}+\mathbf{v}\nabla)];$$

energy conservation:

$$\rho C_p\left[\frac{\partial T}{\partial t}+(\mathbf{v}\cdot\nabla)T-\nabla_{\mathrm{ad}}\frac{T}{P}\left(\frac{\partial P}{\partial t}+(\mathbf{v}\cdot\nabla)P\right)\right] = -\nabla\cdot\mathbf{F}+\Phi,$$

where the rate of viscous dissipation

$$\Phi = \tfrac{1}{2}\mu(\nabla\mathbf{v}+\mathbf{v}\nabla)\cdot(\nabla\mathbf{v}+\mathbf{v}\nabla)-\tfrac{2}{3}\mu(\nabla\cdot\mathbf{v})^2 .$$

We treat the medium as a perfect gas undergoing ionization and we include in P the contribution due to the radiation pressure, but neglect that due to the turbulent pressure. We have adopted the following chemical composition: $X = 0.706$, $Y = 0.280$, and $Z = 0.013$ and have considered all the stages of ionization for various elements with the help of Saha's ionization equations. In the foregoing equations μ is the coefficient of dynamic viscosity, C_p is the specific heat at constant pressure, ∇_{ad} is the logarithmic adiabatic gradient, $(\partial \ln T/\partial \ln P)_{\mathrm{ad}}$ and $\mathbf{F}$ is the total flux which is sum of the radiative flux, $\mathbf{F}^R$ and the convective flux, $\mathbf{F}^C$. The radiative flux is computed in the Eddington approximation by writing (Unno and Spiegel, 1966)

$$\mathbf{F}^R = -\frac{4}{3\kappa\rho}\nabla J,$$

where

$$J = \sigma T^4+\frac{C_p}{4\kappa}\left[\frac{\partial T}{\partial t}+\mathbf{v}\cdot\nabla\mathrm{T}-\nabla_{\mathrm{ad}}\frac{T}{P}\left(\frac{\partial P}{\partial t}+\mathbf{v}\cdot\nabla P\right)\right]$$

is the intensity of radiation and κ the mean Rosseland opacity. In order to compute the convective flux we adopt the standard mixing length formalism and write

$$\mathbf{F}^C = -K_t\left(\nabla T-\nabla_{\mathrm{ad}}\frac{T}{P}\nabla P\right),$$

with the coefficient of turbulent heat conductivity taken to be of the form

$$K_t = \alpha\rho C_p WL .$$

In this expression α is the efficiency factor of order unity, L is the mixing length,

and W the mean convective velocity given by

$$W = \left[\beta \frac{g}{H_p} QL^2(\nabla - \nabla_{ad})\right]^{1/2}.$$

Here β represents the effect of viscous braking on the convective elements, H_p is the pressure scale height, and the factor $Q = -(T/\rho)(\partial\rho/\partial T)_P$ makes allowance for the variation of the degree of ionization in the moving element. The molecular viscosity is negligible compared to the turbulent viscosity and hence it is not considered in the present work. For the turbulent dynamic viscosity we adopt the expression

$$\mu_t = P_t \alpha \rho W L,$$

where the turbulent Prandtl number P_t is treated as a free parameter in the investigation.

We shall adopt the spherical geometry and assume that any physical quantity in the perturbed state can be expressed as

$$f(r, \theta, \phi, t) = f_0(r) + f_1(r) Y_l^m(\theta, \phi)\, e^{\omega t},$$

where the subscripts 0 and 1 respectively refer to the unperturbed and perturbed quantities, (r, θ, ϕ) are the spherical polar coordinates with the radial coordinate r measured from the centre of the Sun, $Y_l^m(\theta, \phi)$ are the spherical harmonics and $\omega = \omega_R + i\omega_I$ the complex eigenvalue. The governing equations are linearized by neglecting the higher order terms in perturbed quantities to get the following system of equations:

$$\omega\rho_1 + \nabla \cdot (\rho_0 \mathbf{v}) = 0,$$

$$\omega\rho_0 \mathbf{v} = \rho_1 \mathbf{g} - \nabla P_1 - \tfrac{2}{3}\mu_{t0}\nabla(\nabla \cdot \mathbf{v}) - \tfrac{2}{3}(\nabla \cdot \mathbf{v})\nabla\mu_{t0} + \nabla \cdot [\mu_{t0}(\nabla\mathbf{v} + \mathbf{v}\nabla)],$$

$$\rho_0 C_{P0}\left[\omega T_1 + (\mathbf{v} \cdot \nabla)T_0 - \nabla_{ad}\frac{T_0}{P_0}(\omega P_1 + (\mathbf{v} \cdot \nabla)P_0)\right] = -\nabla \cdot \mathbf{F}_1,$$

$$\mathbf{F}_1 = -\frac{4}{3\kappa_0\rho_0}\nabla J_1 - \mathbf{F}_0^R\frac{\kappa_1}{\kappa_0} - \mathbf{F}_0^R\frac{\rho_1}{\rho_0} -$$

$$-K_{t0}\left[\nabla T_1 - \nabla_{ad}\frac{T_0}{P_0}\nabla P_1 - \left(\nabla_{ad}\frac{T}{P}\right)_1 \nabla P_0\right] - K_{t1}\left(\nabla T_0 - \nabla_{ad}\frac{T_0}{P_0}\nabla P_0\right),$$

$$J_1 = 4\sigma T_0^3 T_1 + \frac{C_{P0}}{4\kappa_0}\left[\omega T_1 + (\mathbf{v} \cdot \nabla)T_0 - \nabla_{ad}\frac{T_0}{P_0}(\omega P_1 + (\mathbf{v} \cdot \nabla)P_0)\right].$$

In these equations

$$\frac{K_{t1}}{K_{t0}} = \frac{\rho_1}{\rho_0} + \frac{C_{p1}}{C_{p0}} + 2\frac{L_1}{L_0} + \frac{1}{2}\frac{Q_1}{Q_0} - \frac{1}{2}\frac{T_1}{T_0} +$$

$$+\frac{1}{2}\frac{\dfrac{dT_1}{dr} - \left(\nabla_{ad}\dfrac{T}{P}\right)_0\dfrac{dP_1}{dr} - \left(\nabla_{ad}\dfrac{T}{P}\right)_1\dfrac{dP_0}{dr}}{\dfrac{dT_0}{dr} - \nabla_{ad}\dfrac{T_0}{P_0}\dfrac{dP_0}{dr}},$$

$$\frac{L_1}{L_0} = 0$$

for models (A) and (B) discussed in the next subsection, and

$$= \frac{P_1}{P_0} + \frac{1}{\rho_0 g_0}\frac{\mathrm{d}P_1}{\mathrm{d}r}$$

for model (C), while κ, ρ, C_p, Q, $(\nabla_{\mathrm{ad}}(T/P))$ being functions of T and P alone their perturbations can be expressed in the form

$$f_1 = \left(\frac{\partial f}{\partial P}\right)_T P_1 + \left(\frac{\partial f}{\partial T}\right)_P T_1 ,$$

where f can be any one of these quantities, and

$$\mathbf{F}_0^R = -\frac{16\sigma T_0^3}{3\kappa_o \rho_0}\nabla T_0$$

is the radiative flux in the unperturbed state.

We choose the velocity perturbation $\mathbf{v}(r, \theta, \phi)$ and the flux perturbation $\mathbf{F}_1(r, \theta, \phi)$ to have the form

$$\mathbf{v}(r, \theta, \phi) = \left(v_r(r), v_h(r)\frac{\partial}{\partial\theta}, v_h(r)\frac{1}{\sin\theta}\frac{\partial}{\partial\phi}\right) Y_l^m(\theta, \phi) ,$$

$$\mathbf{F}_1(r, \theta, \phi) = \left(F_r(r), F_h(r)\frac{\partial}{\partial\theta}, F_h(r)\frac{1}{\sin\theta}\frac{\partial}{\partial\phi}\right) Y_l^m(\theta, \phi) .$$

This enables us to separate the governing equations into radial and horizontal components, which after some algebraic manipulation, can be cast in the following form with z measured downwards from the level of optical depth unity:

$$\frac{4}{3}\mu_{t0}\frac{\mathrm{d}^2 v_r}{\mathrm{d}z^2} + \frac{\mathrm{d}P_1}{\mathrm{d}z} = \left[\frac{8}{3}\frac{\mu_{t0}}{r^2} + \mu_{t0}\frac{l(l+1)}{r^2} - \frac{4}{3r}\frac{\mathrm{d}\mu_{t0}}{\mathrm{d}z} + \rho_0\omega\right] v_r +$$

$$+ \left[\frac{8}{3}\frac{\mu_{t0}}{r} - \frac{4}{3}\frac{\mathrm{d}\mu_{t0}}{\mathrm{d}z}\right]\frac{\mathrm{d}v_r}{\mathrm{d}z} + \frac{l(l+1)}{r}\left[\frac{2}{3}\frac{\mathrm{d}\mu_{t0}}{\mathrm{d}z} - \frac{7}{3}\frac{\mu_{t0}}{r}\right] v_h -$$

$$- \frac{l(l+1)}{3r}\mu_{t0}\frac{\mathrm{d}v_h}{\mathrm{d}z} + g\left(\frac{\partial\rho}{\partial P}\right)_T P_1 + g\left(\frac{\partial\rho}{\partial T}\right)_P T_1 ,$$

$$\mu_{t0}\frac{\mathrm{d}^2 v_h}{\mathrm{d}z^2} = \left[\frac{1}{r}\frac{\mathrm{d}\mu_{t0}}{\mathrm{d}z} - \frac{8}{3}\frac{\mu_{t0}}{r^2}\right] v_r + \frac{\mu_{t0}}{3r}\frac{\mathrm{d}v_r}{\mathrm{d}z} +$$

$$+ \left[\frac{4}{3}\frac{l(l+1)}{r^2}\mu_{t0} - \frac{1}{r}\frac{\mathrm{d}\mu_{t0}}{\mathrm{d}z} + \omega\rho_0\right] v_h +$$

$$+ \left[\frac{2}{r}\mu_{t0} - \frac{\mathrm{d}\mu_{t0}}{\mathrm{d}z}\right]\frac{\mathrm{d}v_h}{\mathrm{d}z} + \frac{1}{r}P_1 ,$$

We shall also consider different forms of the viscosity coefficient by varying the exponent n in the expression

$$\nu_t = P_t \alpha WL \quad \text{for} \quad t_c < P$$
$$= P_t \alpha WL (P/t_c)^n \quad \text{for} \quad t_c \gg P ,$$

and examine the sensitivity of numerical results to the choice of ν_t.

C. BOUNDARY CONDITIONS

The equations governing the perturbed quantities form a set of six first-order differential equations, and these are solved as characteristic-value problem with the complex eigenvalue ω, by specifying six boundary conditions, three at each interface. The eigenvalues were computed with two different sets of boundary conditions.

(I) Free-boundary conditions at the inner and outer boundaries at which the Lagrangian pressure perturbation vanishes and also the tangential components of the viscous stress tensor vanish, that is,

$$\omega P_1 - g\rho_0 v_r = 0 ,$$

$$v_r + r\frac{\mathrm{d}v_h}{\mathrm{d}r} - v_h = 0 .$$

In addition, the thermal condition requiring the radiation not to come into the layer from infinity, is imposed at the upper boundary; i.e.

$$\frac{v_r}{\omega}\left(\frac{4}{T_0}\frac{\mathrm{d}T_0}{\mathrm{d}r} + \frac{2}{r}\right) + \frac{J_1}{\sigma T_0^4} - \frac{F_r}{F_0^R} = 0 .$$

At the lower boundary we demand the vanishing of Lagrangian perturbation in flux, i.e.

$$\frac{F_r}{F_0^R} - \frac{2}{r}\frac{v_r}{\omega} = 0 .$$

(II) The mechanical and thermal conditions adopted by Ando and Osaki (1975) at the outer boundary along with the vanishing of the viscous stress tensor. In our notation, the mechanical condition becomes

$$(\beta - V_G + 3)x - (\eta - V_G)p = 0 ,$$

where

$$x = v_r/(r\omega) , \qquad p = P_1/(\rho_0 g r) ,$$

$$\eta = -\frac{l(l+1)}{r\omega^2} g ,$$

$$V_G = \left[\left(\frac{\partial\rho}{\partial P}\right)_T + \left(\frac{\partial\rho}{\partial T}\right)_P \nabla_{\mathrm{ad}} \frac{T_0}{P_0}\right] g r ;$$

There is an overshoot of motion from the subphotospheric layers into the bounding region. The variation of the observed velocity field with height given by Canfield (1976) suggests that the amplitude of granular velocities is an exponentially decreasing function with an approximate scale-height of 150 km. We estimate the coefficient of dynamic viscosity in the atmosphere by assuming a Kolmogoroff spectrum with turbulent velocities proportional to the one-third power of the scale-length. With the allowance for the almost exponential fall of density with height, we find that the coefficient of viscosity drops exponentially with a scale height of 25 km. In the layer below the convection zone the coefficient of viscosity is taken to have a constant value since the overshoot into the deeper regions is expected to have a negligible influence on the stability characteristics.

We shall follow the customary approach in fluid mechanics by envisaging the turbulent flow as a superposition of eddies and represent the effect of turbulence on large-scale motions through an eddy viscosity. We shall adopt for this purpose the form for the coefficient of turbulent viscosity given by Goldreich and Keeley (1977) where the dominant contribution to the excitation of a normal mode is supposed to arise from those turbulent eddies whose turn-over times t_c are comparable to the period of oscillation of the mode P. Near the top of the convection zone the turn-over time $t_c = L/W$ is shorter than the period of oscillation and the dominant driving comes from the eddies which have characteristic size L and mean velocity W. For example at a depth of 20 km velocity $W \simeq 3$ km s^{-1}, mixing length $L \simeq 500$ km and hence $t_c \simeq 160$ s which is shorter than the typical period of oscillation ($\simeq$300 s). In the deeper regions of the convection zone the turnover times are much longer than the period of oscillation of the normal modes and the turbulent eddies will cover in such a time distances short compared to the mixing length, thus lowering the efficiency of turbulent viscosity. Thus most of the excitation is supposed to arise from the resonant eddies with scale-size $\lambda (\ll WL)$ for which $t_\lambda = \lambda / W_\lambda$ is comparable with P. We can write the coefficient of turbulent viscosity as

$$\begin{aligned} \nu_t &= P_t \alpha WL \quad \text{for} \quad t_c < P \\ &= P_t \alpha W_\lambda \lambda \quad \text{for} \quad t_c \gg P . \end{aligned}$$

Assuming the Kolmogoroff scaling to be applicable for turbulent eddies of size λ, we can express the eddy velocity by $W_\lambda = W(\lambda/_L)^{1/3}$ and the eddy life-time by $t_\lambda = t_c(\lambda/L)^{2/3}$ to get the coefficient of eddy viscosity in the form

$$\nu_t = P_t \alpha WL (t_\lambda / t_c)^2 .$$

With the main contribution to the excitation arising from the eddies that are in resonance with oscillations, that is, for those with $t_\lambda \simeq P$ we can express the coefficient of viscosity as

$$\begin{aligned} \nu_t &= P_t \alpha WL \quad \text{for} \quad t_c < P \\ &= P_t \alpha WL (P/t_c)^2 \quad \text{for} \quad t_c \gg P . \end{aligned}$$

$$\frac{dF_r}{dz} = -\rho_0^2 C_{p0} g \frac{T_0}{P_0}(\nabla - \nabla_{ad}) v_r - \nabla_{ad} \frac{T_0}{P_0}\left(\omega \rho_0 C_{p0} + \frac{l(l+1)}{r^2} K_{t0}\right) P_1 +$$

$$+\left(\omega \rho_0 C_{p0} + \frac{l(l+1)}{r^2} K_{t0}\right) T_1 + \frac{2}{r} F_r + \frac{l(l+1)}{r^2} \frac{4}{3\kappa_0 \rho_0} J_1 ,$$

$$K_{t0} \frac{dT_1}{dz} - K_{t0} \nabla_{ad} \frac{T_0}{P_0} \frac{dP_1}{dz} - K_{t0}\left(\nabla_{ad} \frac{T}{P}\right)_1 \frac{dP_0}{dz} + K_{t1} \frac{dT_0}{dz} -$$

$$-K_{t1} \nabla_{ad} \frac{T_0}{P_0} \frac{dP_0}{dz} + \frac{4}{3\kappa_0 \rho_0} \frac{dJ_1}{dz} = F_r + F_0^R\left(\frac{\kappa_1}{\kappa_0} + \frac{\rho_1}{\rho_0}\right) ,$$

$$\left(\frac{1}{\rho_0} \frac{d\rho_0}{dz} - \frac{2}{r}\right) v_r + \frac{dv_r}{dz} + \frac{l(l+1)}{r} v_h - \frac{\omega}{\rho_0}\left(\frac{\partial \rho}{\partial P}\right)_T P_1 - \frac{\omega}{\rho_0}\left(\frac{\partial \rho}{\partial T}\right)_P T_1 = 0 ,$$

$$\frac{g \rho_0 T_0 C_{p0}}{4\kappa_0 P_0}(\nabla - \nabla_{ad}) v_r + \nabla_{ad} \frac{\omega T_0 C_{p0}}{4\kappa_0 P_0} P_1 - \left(4\sigma T_0^3 + \frac{\omega C_{p0}}{4\kappa_0}\right) T_1 + J_1 = 0 .$$

Thus the system of governing equations can be written as six first order differential equations along with two auxiliary equations.

B. EQUILIBRIUM SOLAR MODELS

The five-minute oscillations (with $\omega_I \simeq 0.02\ \mathrm{s}^{-1}$) can be analysed as a purely atmospheric phenomenon (Ando and Osaki, 1975). It is, therefore, sufficient to consider only the convection zone of the sun and the overlying atmospheric layers. We have adopted three equilibrium solar envelope models for studying the instability of acoustic modes. The main requirement for the models is that the physical variables at the base of the convection zone should match with the interior solutions and they should also be consistent with the evolutionary computation which can generate the present solar radius and luminosity. We have used Spruit's (1977) model which is constructed with the mixing-length parameters $\alpha = \frac{1}{4}$, $\beta = \frac{1}{8}$, $Q = 1$, and the mixing length $L = z + 459$ km (z being measured downwards from the top of the convection zone). In addition, we have used the following two solar envelope models as the basic state for analysing the instability of acoustic modes:

$$\alpha = \tfrac{1}{4}, \quad \beta = \tfrac{1}{8}, \quad Q \neq 1 \quad \text{and} \quad L = \zeta + 459\ \mathrm{km} ,$$

$$\alpha = \tfrac{1}{3}, \quad \beta = \tfrac{1}{8}, \quad Q \neq 1 \quad \text{and} \quad L = 2.5\, H_p .$$

For the atmosphere we have adopted the empirical temperature-optical depth ($T - \tau$) relationship given by Vernazza *et al.* (1976), with the upper boundary chosen a little below the temperature minimum at a level where $\tau = 7 \times 10^{-4}$; the lower boundary for the layer is fixed at a depth of $\simeq 4 \times 10^5$ km ($T \simeq 5 \times 10^6$ K). The equilibrium run of the physical quantities was generated by integrating the standard structure equations and the partial derivatives $(\partial\rho/\partial P)_T$, $(\partial\rho/\partial T)_P$ were calculated with the help of the equation of state for a perfect gas undergoing ionization. The partial derivatives of the opacity, $(\partial\kappa/\partial T)_P$, $(\partial\kappa/\partial P)_T$ were computed making use of the opacity tables given by Cox and Stewart (1970).

$\beta_{\pm}$ are solutions of the quadratic equation

$$\beta^2-(A+V_G-2)\beta+\left(\eta A-\frac{r\omega^2}{g}V_G+V_G-l(l+1)-3A-3\right)=0\,,$$

where

$$A=\left(\frac{\partial\rho}{\partial T}\right)_P(\nabla-\nabla_{\mathrm{ad}})\frac{T_0}{P_0}rg\,.$$

The thermal condition and the condition on the vanishing of the tangential component of the viscous stress are the same as in (*I*), namely,

$$\frac{V_r}{\omega}\left(\frac{4}{T_0}\frac{\mathrm{d}T_0}{\mathrm{d}r}+\frac{2}{r}\right)+\frac{J_1}{\partial T_0^4}-\frac{F_r}{F_0^R}=0\,,$$

$$V_r+r\frac{\mathrm{d}V_h}{\mathrm{d}r}-V_h=0\,.$$

At the lower surface the conditions are the same as in (I).

D. NUMERICAL TECHNIQUE

The system of equations along with the sets of boundary conditions (I) or (II) form a generalized eigenvalue problem with complex eigenvalues and complex eigenfunctions to be determined for a specified value of the horizontal harmonic number *l*. In order to solve these equations we have used a finite-difference scheme with explicit calculation of the first-order corrections (Antia, 1979). The resultant matrix is solved to obtain complex eigenvalues by the Muller iteration method. The initial guess for the eigenvalue is made by solving the equations under non-viscous, adiabatic conditions and the adiabatic eigenvalue is fed as the starting value for the iteration. The iteration is continued until the complex eigenvalue obtained is accurate to less than 1 part in 10^5. The complex eigenfunction is calculated by appealing to the inverse iteration method (Wilkinson, 1965). The first-order correction for the eigenfrequency was found to be less than one percent, while the correction to the growth rate was at most 5%. We have taken 121 mesh points inside the convection zone and 30 points covering the atmospheric region. The computations were performed on DEC system 1077 with single precision arithmetic.

3. Numerical Results

We have solved the system of equations governing viscous non-adiabatic non-radial oscillations to obtain the complex eigenvalues for a specified value of the horizontal harmonic number *l*. The horizontal wavelength of the eigenmode is then given by

$$\lambda=\frac{2\pi}{k_h}=\frac{2\pi R_\odot}{\sqrt{l(l+1)}}\,,$$

where k_h is the horizontal wave number and $R_\odot$ the solar radius. We get a series

of complex eigenvalues ω for each value of l. The p-modes are characterized by the number of velocity nodes in the radial direction and by the order l, and we refer to the lowest eigenfrequency, the fundamental mode, as p_0-mode, and the successive harmonics $p_1, p_2, p_3, \ldots$.

We shall be concerned with the study of non-radial solar oscillations with periods predominantly in the neighbourhood of 300 s. The bulk of these oscillations are not expected to penetrate deeper regions of the Sun and at any rate the amplitudes of the eigenfunctions decay sharply below the depth of a few tens of thousand kilometers. Consequently the inner boundary conditions do not have an appreciable effect on the stability characteristics of acoustic modes. However, there is a considerable penetration of the p-modes into the overlying layers and the eigenfunctions in fact approach their peak values in the solar atmosphere. The outer boundary conditions have, as a result, a significant influence on the growth rates of acoustic modes.

The main objective of the present investigation is to compare the characteristics of the most unstable modes excited in a solar envelope model with the observed features of not only granulation and supergranulation, but also those associated with the five-minute oscillations. Since the turbulent Prandtl number, P_t is treated as a free parameter in our work, we first examine the stability of convective modes for the three envelope models, (A), (B), and (C) with a view to fix the values of P_t. Table I shows the approximate e-folding times and preferred horizontal wavelengths corresponding to the most rapidly growing fundamental mode and the first harmonic for the three models. The turbulent Prandtl number is so chosen in each case as to reproduce the most reasonable agreement with the granular and supergranular motions. Thus, for model (A), the choice of $P_t = \frac{1}{3}$ yields the e-folding time and the preferred horizontal wavelength of the most unstable fundamental mode (C_1) and the first harmonic (C_2) which are in reasonable accord respectively with the life-times and length-scales corresponding to granulation and supergranula-

TABLE I

Approximate e-folding times and preferred horizontal wavelengths corresponding to the most unstable fundamental mode (C_1) and the first harmonic (C_2) for the solar envelope models (A), (B), and (C). The values of physical variable for each model refers to the base of convection zone

Model	Mixing length parameters			Physical variables				Fundamental mode (C_1)		First harmonic (C_2)	
	α	β	L	Depth (km)	ρ_{base} (g cm^{-3})	T_{base} (10^6 K)	P_t	e-folding time (min)	Preferred horizontal wavelength (km)	e-folding time (hr)	Preferred horizontal wavelength (km)
(A)	$\frac{1}{4}$	$\frac{1}{8}$	$z+459$ km	19 600	0.250	2.18	$\frac{1}{3}$	9.6	2400	32.0	11 000
	$Q \neq 1$										
(B)	$\frac{1}{4}$	$\frac{1}{8}$	$z+459$ km	19 200	0.228	2.18	$\frac{1}{2}$	8.6	2450	15.0	9 000
	$Q = 1$ (Spruit)										
(C)	$\frac{1}{3}$	$\frac{1}{8}$	$2.5H_p$	19 800	0.272	2.185	$\frac{2}{3}$	11.9	3050	34.8	11 400

tion. Likewise, for models (B) and (C) the values of $P_t = \frac{1}{2}$ and $\frac{2}{3}$ respectively, produce the desired results.

We employ these values of the turbulent Prandtl numbers to investigate the stability of non-radial acoustic modes in the three solar envelope models. First, let us examine the standard case considered by Ando and Osaki (1975) and by Ulrich and Rhodes (1977), and neglect the interaction between convection and oscillation, that is, we take $K_{t0} = 0$, $\mu_{t0} = 0$, and consider only the effect due to the radiative conductivity. The resulting system of equations is then equivalent to that given by Ando and Osaki. We use model (A) for the basic state and adopt the set of boundary conditions (I) without the requirement of the vanishing of the viscous stress tensor. The results are summarized in Table II showing (i) harmonic number l, (ii) horizontal wave number k_h (Mm^{-1}), (iii) the mode number, (iv) the period of oscillation, $P = 2\pi/\omega_I$ (s), (v) the frequency of oscillation, ω_I (s^{-1}), and (vi) the stability coefficient, $\eta = \omega_R/\omega_I$. The numerical results are in satisfactory agreement with those obtained by Ando and Osaki (1975) and also with those by Ulrich and Rhodes (1977). The growth rates are found to be larger than those obtained by Ando and Osaki, but not as large as indicated by Ulrich and Rhodes. The difference of some few percent in the growth rates may be attributed to the choice of the solar envelope model employed to describe the equilibrium state. In fact even our equations are slightly different, since Ando and Osaki have neglected the Lagrangian perturbation in convective flux, while we neglect the Eulerian perturbation. Our results reproduce the pattern of instability showing a long mountain-range like structure. For each harmonic number l, there exists a maximum value of the stability coefficient η with its associated frequency, $(\omega_I)_{\max}$. The locus of the $(\omega_I)_{\max}$ runs horizontally along a line with a period around 300 s upto $l = 200$ turning upwards for large l.

Next, we consider thermal coupling between convection and oscillation by including the effects of turbulent heat conductivity, but neglect the mechanical effects arising from the turbulent viscosity, that is we take $K_{t0} \neq 0$, but set $\mu_{t0} = 0$ ($P_t = 0$). In this case the system of equations is of the fourth order and we adopt the set of boundary conditions (I) without the condition of vanishing of the viscous stress tensor. The η values for this case are shown in the last column of Table II. The period of oscillation is practically unaffected and hence is not shown separately.

The remarkable feature is that the strength of the instability is pronouncedly increased; all the modes are seen to be overstabilized. The growth rate for $l = 200$, for most unstable acoustic mode, P_6, for example, is larger by nearly a factor of 4 over the corresponding growth rate without turbulent conductivity. This clearly demonstrates the influence of turbulent heat conductivity, K_t in rendering the acoustic modes unstable. We shall return to the discussion of the driving mechanism due to the turbulent conduction later in the next section.

Let us now consider the effect of turbulent viscosity on the stability of acoustic modes. Table III summarizes the numerical results for the horizontal harmonic number l ranging from 100 to 1000. It is at once clear, from a comparison of the stability coefficient shown in Tables II and III, that the turbulent viscosity has a

TABLE II

Stability coefficients and eigenfrequencies of nonradial acoustic modes for the solar envelope model (A) for the inviscid case. The values of η in column (a) are obtained by neglecting the turbulent heat conductivity (K_t) while those in column (b) are obtained by taking into account K_t

l	k_h (Mm^{-1})	Mode	Period (s)	ω_I (s^{-1})	η(a)	η(b)
100	0.14	P0	985	6.377 (−3)	−2.039 (−7)	2.258 (−6)
		P1	669	9.388 (−3)	−7.033 (−6)	5.719 (−5)
		P2	541	1.162 (−2)	−8.149 (−6)	2.959 (−4)
		P3	461	1.362 (−2)	2.453 (−5)	7.147 (−4)
		P4	408	1.542 (−2)	1.131 (−4)	1.326 (−3)
		P5	366	1.714 (−2)	2.267 (−4)	1.776 (−3)
		P6	335	1.876 (−2)	3.616 (−4)	2.161 (−3)
		P7	309	2.040 (−2)	4.621 (−4)	1.963 (−3)
		P8	287	2.190 (−2)	5.194 (−4)	2.242 (−3)
		P9	268	2.343 (−2)	5.478 (−4)	2.303 (−3)
		P10	252	2.495 (−2)	5.052 (−4)	2.111 (−3)
		P11	237	2.647 (−2)	3.638 (−4)	1.711 (−3)
		P12	226	2.785 (−2)	1.483 (−4)	1.362 (−3)
		P13	215	2.929 (−2)	−1.434 (−4)	1.023 (−3)
200	0.29	P0	702	8.954 (−3)	−5.042 (−7)	6.334 (−6)
		P1	507	1.239 (−2)	−4.831 (−6)	7.847 (−4)
		P2	413	1.521 (−2)	1.171 (−4)	1.632 (−3)
		P3	356	1.766 (−2)	3.632 (−4)	2.719 (−3)
		P4	313	2.010 (−2)	4.836 (−4)	3.447 (−3)
		P5	282	2.232 (−2)	7.413 (−4)	3.347 (−3)
		P6	257	2.446 (−2)	7.472 (−4)	3.144 (−3)
		P7	237	2.652 (−2)	5.373 (−4)	2.535 (−3)
		P8	220	2.885 (−2)	1.012 (−4)	1.773 (−3)
		P9	206	3.052 (−2)	−5.591 (−4)	1.019 (−3)
400	0.57	P0	499	1.260 (−2)	−3.005 (−7)	2.294 (−5)
		P1	385	1.632 (−2)	1.807 (−4)	2.243 (−3)
		P2	317	1.985 (−2)	7.703 (−4)	4.699 (−3)
		P3	270	2.330 (−2)	1.157 (−3)	5.282 (−3)
		P4	237	2.656 (−2)	9.424 (−4)	4.281 (−3)
		P5	213	2.951 (−2)	6.843 (−6)	2.136 (−3)
600	0.86	P0	408	1.541 (−2)	2.194 (−6)	4.484 (−5)
		P1	322	1.949 (−2)	5.787 (−4)	4.176 (−3)
		P2	266	2.358 (−2)	1.300 (−3)	6.095 (−3)
		P3	228	2.756 (−2)	1.075 (−3)	5.160 (−3)
		P4	201	3.133 (−2)	−7.007 (−4)	2.295 (−3)
800	1.14	P0	354	1.777 (−2)	6.618 (−6)	6.281 (−5)
		P1	281	2.237 (−2)	1.053 (−3)	5.691 (−3)
		P2	233	2.697 (−2)	1.406 (−3)	6.206 (−3)
		P3	201	3.130 (−2)	−3.471 (−4)	3.204 (−3)
1000	1.43	P0	316	1.985 (−2)	1.171 (−5)	7.329 (−5)
		P1	250	2.510 (−2)	1.462 (−3)	6.602 (−3)
		P2	208	3.024 (−2)	3.192 (−4)	5.011 (−3)

TABLE III

Stability coefficients and eigenfrequencies of nonradial acoustic modes for solar envelope model (A) with the turbulent heat conductivity and turbulent viscosity included. Here the turbulent Prandtl number $P_t = \frac{1}{3}$

l	k_h (Mm^{-1})	Mode	Period (s)	ω_I (s^{-1})	η
100	0.14	P0	1003	6.262 (−3)	−4.497 (−5)
		P1	677	9.278 (−3)	−1.460 (−5)
		P2	546	1.151 (−2)	8.478 (−5)
		P3	464	1.353 (−2)	3.208 (−4)
		P4	411	1.531 (−2)	5.281 (−4)
		P5	367	1.711 (−2)	7.736 (−4)
		P6	335	1.873 (−2)	9.537 (−4)
		P7	310	2.024 (−2)	1.009 (−3)
		P8	287	2.186 (−2)	9.891 (−4)
		P9	269	2.340 (−4)	9.873 (−4)
		P10	252	2.494 (−2)	9.341 (−4)
		P11	239	2.633 (−2)	5.663 (−4)
		P12	226	2.779 (−2)	3.170 (−5)
		P13	215	2.921 (−2)	−1.145 (−5)
200	0.29	P0	714	8.795 (−3)	−1.711 (−4)
		P1	513	1.224 (−2)	−5.666 (−5)
		P2	416	1.509 (−2)	4.330 (−4)
		P3	357	1.758 (−2)	1.029 (−3)
		P4	315	1.996 (−2)	1.499 (−3)
		P5	281	2.234 (−2)	1.465 (−3)
		P6	257	2.445 (−2)	1.356 (−3)
		P7	237	2.646 (−2)	8.171 (−4)
		P8	221	2.848 (−2)	1.648 (−4)
		P9	206	3.049 (−2)	−6.108 (−4)
400	0.57	P0	507	1.239 (−2)	−1.259 (−3)
		P1	389	1.617 (−2)	−5.440 (−4)
		P2	318	1.977 (−2)	1.174 (−3)
		P3	270	2.324 (−2)	1.781 (−3)
		P4	237	2.656 (−2)	1.417 (−3)
		P5	213	2.946 (−2)	−1.084 (−5)
600	0.86	P0	414	1.518 (−2)	−3.886 (−3)
		P1	325	1.936 (−2)	−1.034 (−3)
		P2	267	2.351 (−2)	1.246 (−3)
		P3	228	2.758 (−2)	1.189 (−3)
		P4	201	3.129 (−2)	−1.099 (−3)
800	1.14	P0	358	1.755 (−2)	−7.749 (−3)
		P1	282	2.228 (−2)	−1.545 (−3)
		P2	233	2.696 (−2)	8.593 (−4)
		P3	201	3.126 (−2)	−1.126 (−3)
1000	1.43	P0	320	1.965 (−2)	−1.247 (−2)
		P1	251	2.507 (−2)	−1.760 (−3)
		P2	208	3.022 (−2)	−4.652 (−5)

damping effect on the acoustic modes which are manifestly stabilized in relation to the case when the viscosity was absent ($P_t = 0$). Thus, for values of the harmonic number l upto 400, the stability coefficients are lowered by a factor of nearly 3, and the damping effect due to viscosity is even more pronounced for higher values of l and for higher harmonics.

We have also investigated the overstability of acoustic modes of order l ranging from 100 to 1000 for solar envelope models (B) and (C). For lower values of l degree of instability corresponding to the most unstable mode is invariably stronger in model (B) (with $P_t = \frac{1}{2}$) over those obtained in model (A) (with $P_t = \frac{1}{3}$), but for larger values of l the degree of instability is markedly weaker. In the case of envelope model (C) with the higher Prandtl number required to reproduce the characteristic granular features, all the acoustic modes are found to be stabilized. The acoustic modes are highly sensitive to the value of the turbulent Prandtl number and for a choice of $P_t = 1$, in fact, the acoustic modes in all the three models turn out to be stable. The stabilization of the acoustic modes by the effects of turbulent viscosity has been noted earlier by Goldreich and Keeley (1977). We attribute the stability of all the radial p-modes in their work to the uncertainties in the estimate of turbulent damping; a large value of the turbulent Prandtl number ($P_t \simeq 1$) is inherent in their investigation. In all the three models that we considered the fundamental mode is always stable which is consistent with its observed low power. The higher order acoustic modes are presumably stabilized on account of the strong atmospheric radiative dissipation. However, it is interesting to note that the fundamental mode is unstable in the inviscid case (cf. Table II), while it is invariably damped in the presence of viscosity. This could be attributed to the larger amplitudes of the velocity eigenfunctions of the p_0-mode in the deeper regions of the convective zone compared to those associated with the higher harmonics. The viscous dissipation is consequently very effective in damping the p_0-mode which therefore is liable to be stabilized when the viscosity is included.

With a view to test the sensitivity of the results to the form of the coefficient of turbulent viscosity adopted in the calculation ($\nu_t = P_t \alpha WL(P/t_c)^n$), we computed the eigenvalues for the harmonic number $l = 200$ with three values of n, namely $n = 0$, 1, and 2. The results are set out in Table IV, from which it is clearly seen that all the acoustic modes are stable for $n = 0$ case. This choice is a gross overestimate of the viscosity coefficient because, with the period of oscillation small compared to the turnover time, the turbulent eddies will cover a shorter distance than the mixing-length within a cycle of oscillation and this will decrease the efficiency of turbulent viscosity. The acoustic modes become overstable as the exponent n is increased to 1 and a comparison between $n = 1$ and $n = 2$ reveals that the growth rates are lower approximately by a factor of 2 in the former case. This results from the effect of the turbulent viscosity which is lowered with increasing values of the exponent n in the expression of ν_t.

Let us examine the influence of the two sets of boundary conditions: (I) Free foundary conditions, (II) Ando and Osaki's mechanical and thermal conditions.

TABLE IV

Sensitivity of growth rates to the exponent n in the expression $v_t = P_t \alpha WL(P/t_c)^n$ of the viscosity coefficient with $l=200$ for the solar envelope model (A)

Mode	Period (s)	$\eta=\omega_R/\omega_I$		
		$n=0$	$n=1$	$n=2$
P0	714	−5.23 (−3)	−5.61 (−4)	−1.71 (−4)
P1	513	−5.16 (−3)	−6.49 (−4)	−5.67 (−5)
P2	416	−5.00 (−3)	−3.35 (−4)	4.33 (−4)
P3	357	−4.41 (−3)	1.79 (−4)	1.03 (−3)
P4	315	−4.39 (−3)	6.00 (−4)	1.50 (−3)
P5	281	−3.73 (−3)	6.27 (−4)	1.47 (−3)
P6	257	−4.34 (−3)	5.55 (−4)	1.36 (−3)
P7	237	−5.07 (−3)	9.78 (−5)	8.17 (−4)
P8	221	−5.42 (−3)	−4.79 (−4)	1.65 (−4)
P9	206	−6.46 (−3)	−1.22 (−3)	−6.11 (−4)

The results for the two cases are summarized in Table V for the p-modes of degree $l = 200$, with $P_t = \frac{1}{3}$ and the basic equilibrium model (A). The frequencies are practically the same and the stability coefficients are not sensibly different in the two cases except for higher harmonics (beyond p_5). It is also found that the results are not sensitive to the inner boundary conditions where we applied both the rigid as well as the free boundary conditions to get the same growth rates. This is the consequence of the amplitudes of the eigen-functions being small in the deeper

TABLE V

The stability coefficients of non-radial acoustic modes for the solar envelope model (A) for the horizontal harmonic number $l=200$ and $P_t=\frac{1}{3}$ with (I) free boundary conditions, (II) mechanical and thermal conditions adopted by Ando and Osaki

Mode	Period (s)	$\eta=\omega_R/\omega_I$	
		I	II
P0	714	−1.71 (−4)	−1.45 (−4)
P1	513	−5.67 (−5)	−6.73 (−5)
P2	416	4.33 (−4)	4.17 (−4)
P3	357	1.03 (−3)	9.73 (−4)
P4	315	1.50 (−3)	1.49 (−3)
P5	281	1.47 (−3)	1.63 (−3)
P6	257	1.36 (−3)	1.43 (−3)
P7	237	8.17 (−4)	1.11 (−3)
P8	221	1.65 (−4)	5.31 (−4)
P9	206	−6.11 (−4)	−4.83 (−5)

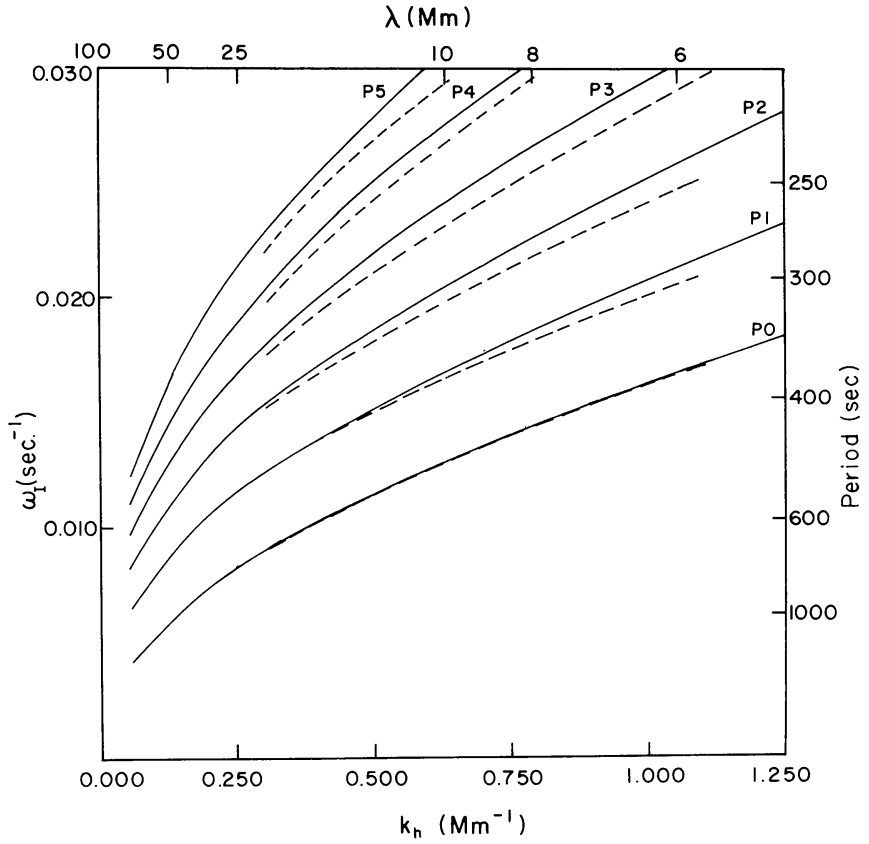

Fig. 1. The frequencies ω_I (s^{-1}) are plotted against the horizontal wave number, k_h (Mm^{-1}) for the first six p-modes calculated with the solar envelope model (A). The eigenfrequencies are labelled by the nodal number n. The dashed lines outline the averaged values of the power ridges taken from Deubner *et al.* (1979).

regions of the convection zone and as a result the growth rates are not sensibly altered.

4. Comparison with Observations and Discussion

We have displayed in Figure 1 the eigenfrequency ω_I (s^{-1}) of various modes as a function of the horizontal wave number k_h (Mm^{-1}). The eigenfrequencies are labelled by p_n, where the nodal number in the radial direction, n, refers to the successive harmonics starting with the fundamental mode p_0. The power of the five-minute oscillations is concentrated in several distinct ridges in the $(k_h - \omega)$-plot. The averaged values of the ridges taken from the recent work of Deubner *et al.* (1979) is shown by the dashed lines. The observed ridges are seen to be in satisfactory agreement with the positions of theoretical nonradial p-modes in the solar envelope model. The overall accordance between the general pattern of observed power ridges and the theoretical power contours is reasonably clear. The theoretical eigenfrequencies of the fundamental mode are in striking agreement with the observed p_0-ridge, but there are noticeable departures between theoretically computed frequencies and observed power spectrum for higher harmonics.

The discrepancies may be attributed to the choice of the solar envelope model and also to the effects arising from the neglect of turbulent pressure and viscous dissipation. The latter would certainly become effective for higher values of l and for higher harmonics. The frequencies of nonradial oscillations calculated in our work, which includes the damping effects due to turbulent viscosity do indeed come out to be lower than the frequencies obtained by Ando and Osaki (1975).

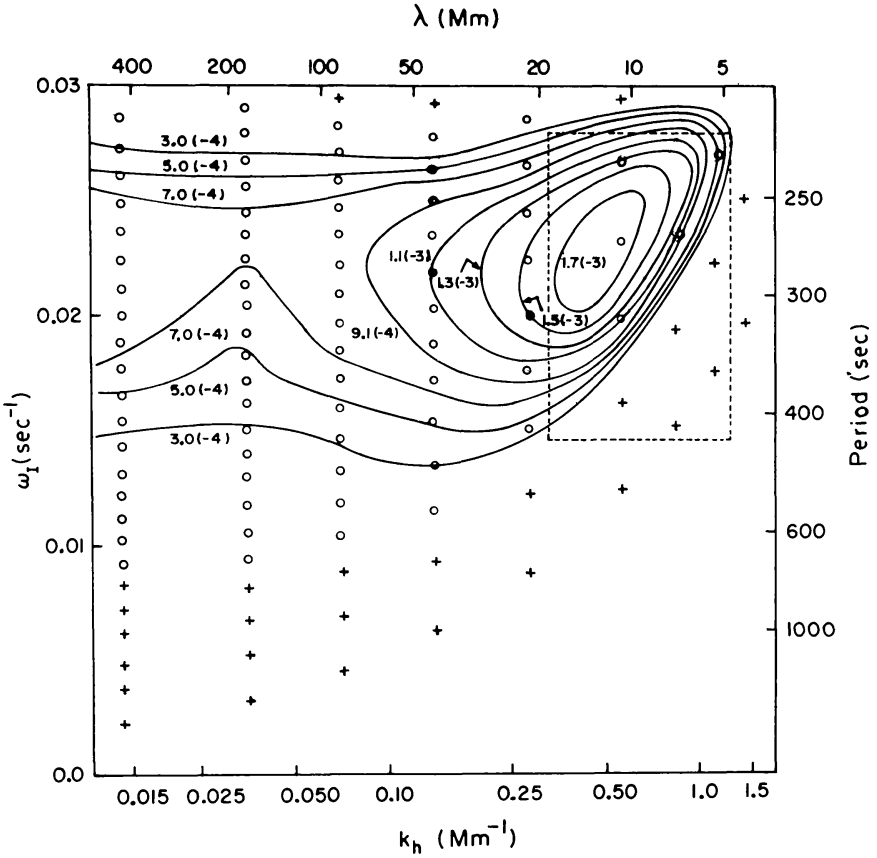

Fig. 2. The diagnostic $(k_h - \omega)$-diagram showing a contour map of equal stability coefficients $\eta = \omega_R/\omega_I$; the stable modes are indicated by crosses and unstable by open circles. The dashed rectangle indicates the region of observed power (Deubner, 1975).

In Figure 2 we have the diagnostic diagram showing a contour map of equal stability coefficients $\eta = \omega_R/\omega_I$, where the stable modes are indicated by crosses and unstable ones by open circles. The region of observed power taken from the work of Deubner (1975) is indicated by a dashed rectangle in the plot. The numbers with parentheses indicating the power of ten denote the values of the stability coefficients. For a given value of l, the growth rate increases with the order of the modes, attains a maximum for a value of the frequency between 0.02 and 0.025 (s^{-1}) and then decreases. This is exhibited by the behaviour of the contour maps of equal η where the locus of $(\omega_I)_{max}$ runs horizontally along a line with a period centred around 300 s up to $l \simeq 400 (k_h \simeq 0.5\ Mm^{-1})$ and then it moves upwards for higher values of l. We have graphed in the companion Figure 3 the plot of the growth rates ω_R (s^{-1}) against the frequency ω_I (s^{-1}) for values of the harmonic

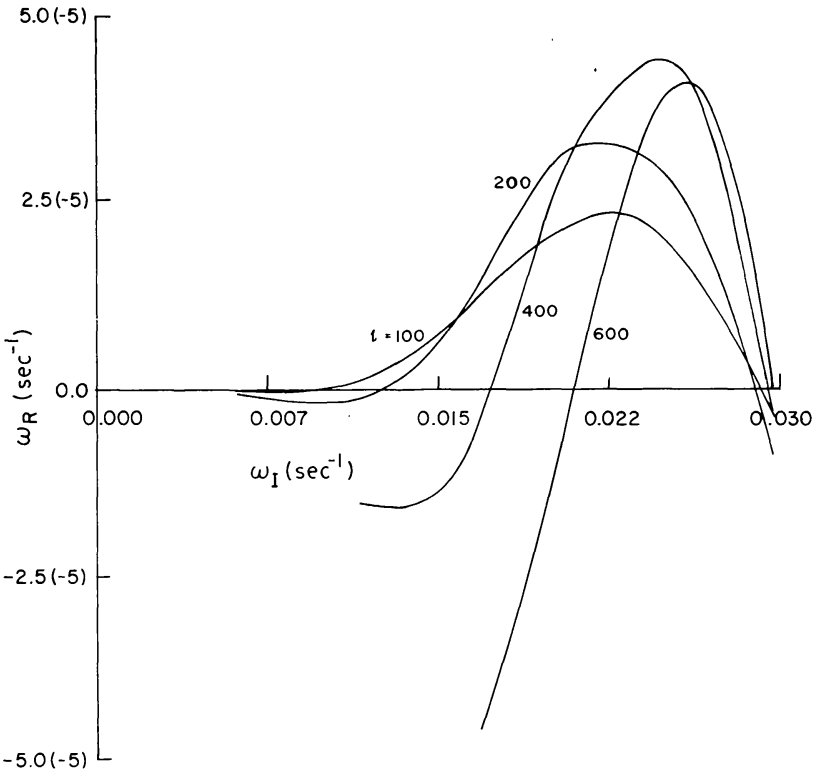

Fig. 3. The growth rate ω_R (s^{-1}) is graphed as a function of the frequency ω_I (s^{-1}) for values of $l = 100$, 200, 400, and 600.

number $l = 100$, 200, 400, and 600. There is a pronounced preferred maximum for ω_R with respect to l around the harmonic number $l = 400$. The overriding value of the maximum stability coefficient, $\eta_{\max} = 1.8 \times 10^{-3}$ for $(\omega_I)_{\max} = 0.023\ s^{-1}$ is situated almost near the central region of the observed rectangle. Clearly its exact location will be influenced by our assumption concerning the form of the viscosity coefficient. The influence of turbulent viscosity is to produce an overall preferred maximum around $l = 400$ because of the increased viscous damping for higher values of the horizontal harmonic number. This feature is absent in the work of Ando and Osaki where because of the neglect of turbulent viscosity, the growth rate of the most unstable mode keeps increasing with l.

In Figure 4 are graphed the cumulative contributions to the normalized kinetic energy of oscillation E_{kin} for p_0, p_3, and p_6-modes of degree $l = 200$. The bumps in the plots of p_3 and p_6-modes result from the nodes in the velocity eigenfunctions, v_r, which are shown in Figure 5. The motions associated with the fundamental mode are spread over a large portion of the outer convection zone penetrating well below the hydrogen ionization zone upto a depth of 30 000 km while those corresponding to the higher order p_3 and p_6-modes are largely concentrated in the surface regions, but the energy of oscillation of these modes is provided by much wider region than for the p_0-mode. In order to understand the mechanisms responsible for destabilization and damping of the solar p-mode oscillations, we display in Figure 6 the normalized rate of change of thermal energy, $\dot{E}_{\text{th}}$, and the rate of

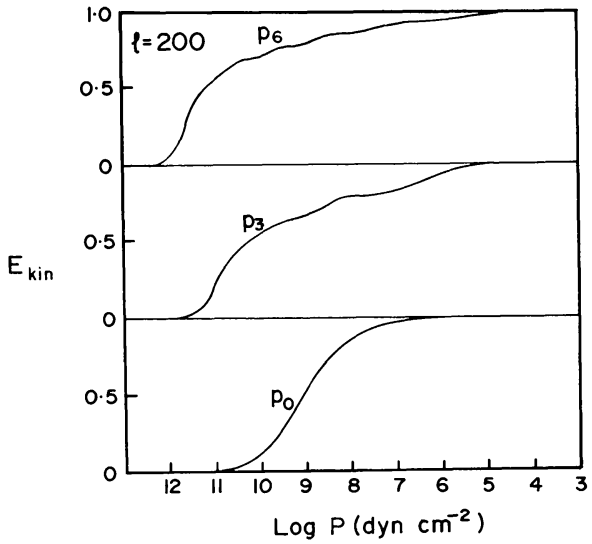

Fig. 4. The cumulative contribution from the bottom of the convection zone to the normalized oscillation energy for p_0, p_3, and p_6-modes, is shown against the logarithm of the pressure. The bumps result from the nodes of velocity eigenfunctions.

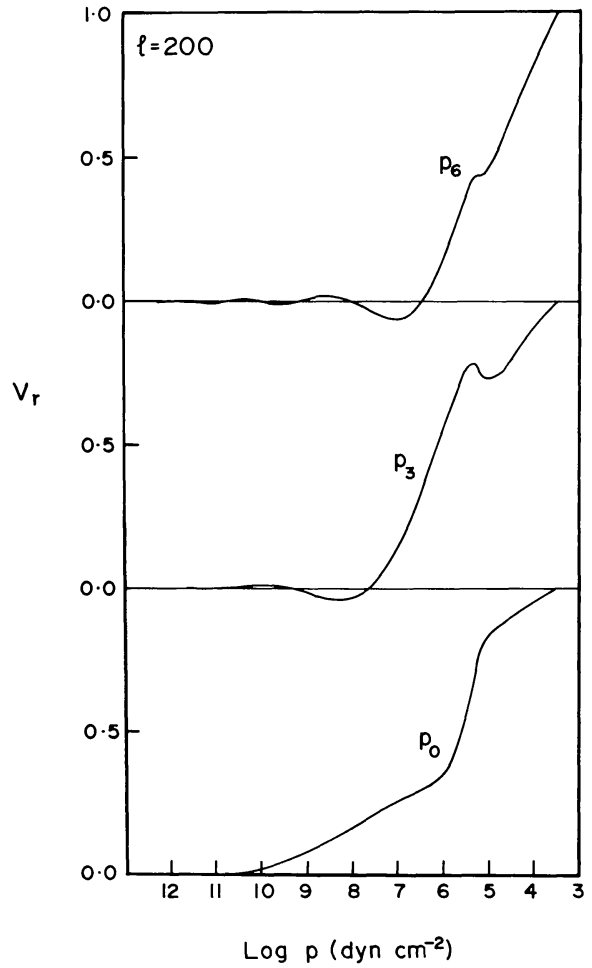

Fig. 5. The radial velocity eigenfunction, v_r is plotted against the logarithm of the pressure for p_0, p_3, and p_6-modes. The velocity is normalized to have a value unity at the outer boundary.

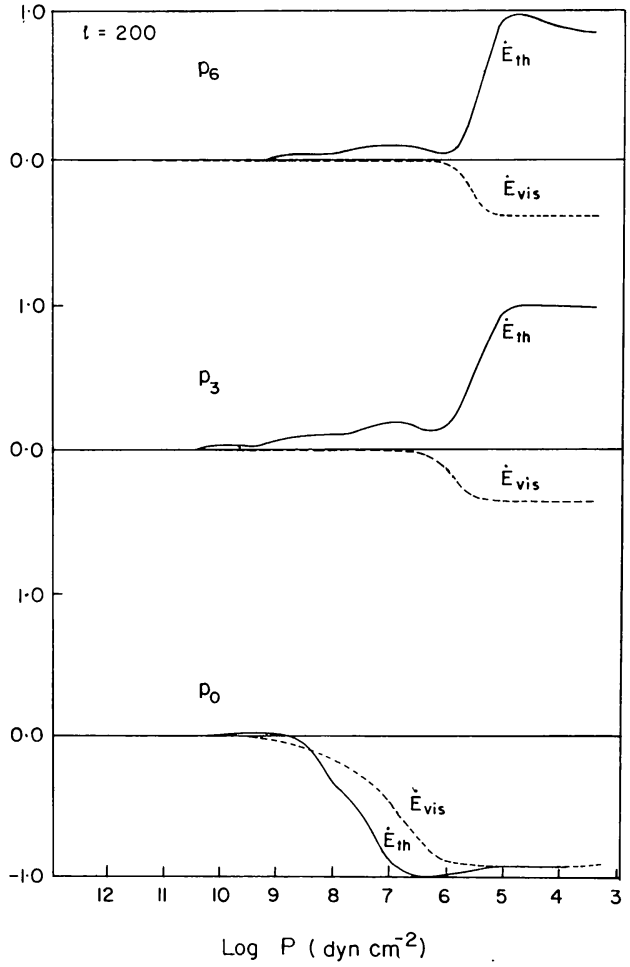

Fig. 6. The normalized rate of change of thermal energy $\dot{E}_{\rm th}$ and the rate of viscous dissipation $\dot{E}_{\rm vis}$ are displayed as a function of log P for p_0, p_3, and p_6-modes.

viscous dissipation, $\dot{E}_{\rm vis}$ as a function of $\log P$ for the p_0, p_3, and p_6-modes of degree $l = 200$. The expressions for $\dot{E}_{\rm th}$ and $\dot{E}_{\rm vis}$ are derived in the Appendix. The slope of these curves determine the contribution to driving or damping of oscillations at a given depth. Clearly the driving of the nonradial oscillations occurs mainly in the sub-photospheric layers where the temperature gradient is strongly superadiabatic. For the case of $l = 200$, the destabilization region extends upto a depth of $\simeq$650 km ($P \simeq 1.5 \times 10^6$ dyn cm^{-2}) for the p_3-mode, and upto $\simeq$500 km ($P \simeq 10^6$ dyn cm^{-2}) for the p_6-mode. The viscous dissipation is spread throughout, although it is more pronounced in the upper portion of the convection zone where the oscillatory velocity field tends to have a large value.

It is clear from the foregoing considerations that the acoustic modes trapped in the solar convection zone are destabilized mainly in the strongly superadiabatic region of the sub-photospheric layers. Two possible mechanisms which have been discussed for the excitation of p-modes in the solar envelope are κ-mechanism and Cowling–Spiegel mechanism operating in the hydrogen ionization zone. It has been

argued by Ando and Osaki (1975) that the κ-mechanism is mainly responsible in driving the five-minute oscillations, although Graff (1976) has pointed out that the Cowling–Spiegel mechanism makes a non-negligible contribution to the generation of acoustic oscillations. The point of view taken by Antia *et al.* (1977) is that a simultaneous action of the κ-mechansim and the Cowling–Spiegel mechanism works to destabilize the solar oscillations, although it was recognized that the radiative Cowling–Spiegel mechanism is a weaker process compared to the κ-mechanism. Unno (1976) was the first to stress the importance of turbulent conduction as an effective mechanism to overstabilize the acoustic modes in the solar envelope. Both the radiative and convective Cowling mechanisms arise on account of the strong superadiabaticity prevailing in the sub-surface regions. But the efficiency of the convective Cowling mechanism turns out to be larger by a factor $(F^C/F^R)(\nabla/(\nabla-\nabla_{ad}))$ compared to the radiative Cowling–Spiegel mechanism. We have incorporated the turbulent conduction (convective Cowling) mechanism through the modulation of the convective flux in the energy equation and have of course included the κ-mechanism and the radiative Cowling-Spiegel mechanism to find that the dominant contribution to the destabilization arises from the turbulent conduction.

This is borne out by our numerical computations. In an attempt to isolate the mechanism responsbile for destabilizing the five-minute oscillations we have shown in Table VI(a, b) the results obtained for nonviscous and viscous layers for the most unstable modes of degree $l = 200$ for two cases: (i) with only the terms arising from the κ-mechanism are retained, while those resulting from the modulation of convective flux are suppressed, (ii) with the κ-mechanism and the full effects of

TABLE VI (a)

The growth rates of non-radial *non-viscous* accoustic modes for the solar envelope model (A) corresponding to $l=200$ when (a) only the κ-mechanism is present and the convective Cowling mechanism is suppressed, (b) when both the κ-mechanism and the convective Cowling mechanism operate

Mode	Period (s)	$\eta=\omega_R/\omega_I$	
		(a)	(b)
P0	702	−5.04 (−7)	6.33 (−6)
P1	507	−4.83 (−6)	7.85 (−4)
P2	413	1.17 (−4)	1.63 (−3)
P3	356	3.63 (−4)	2.72 (−3)
P4	313	4.84 (−4)	3.45 (−3)
P5	282	7.41 (−4)	3.35 (−5)
P6	257	7.47 (−4)	3.14 (−3)
P7	237	5.37 (−4)	2.53 (−3)
P8	220	1.01 (−4)	1.77 (−3)
P9	206	−5.59 (−4)	1.02 (−3)

TABLE VI (b)

The growth rates of non-radial *viscous* acoustic modes for the solar envelope model (A) for $l=200$, with $P_t=\frac{1}{3}$ when (a) only the κ-mechanism operates and the convective Cowling mechanism is suppressed, (b) both k-mechanism and the convective Cowling mechanism operate

Mode	Period (s)	$\eta=\omega_R/\omega_I$	
		(a)	(b)
P0	714	−3.25 (−4)	−1.71 (−4)
P1	513	−4.83 (−4)	−5.67 (−5)
P2	416	−1.03 (−3)	4.33 (−4)
P3	357	−1.11 (−3)	1.03 (−3)
P4	315	−1.34 (−3)	1.50 (−3)
P5	281	−1.48 (−3)	1.47 (−3)
P6	257	−1.66 (−3)	1.36 (−3)
P7	237	−1.72 (−3)	8.17 (−4)
P8	221	−1.78 (−3)	1.65 (−4)
P9	206	−2.54 (−3)	−6.11 (−4)

radiative and turbulent diffusion are included. An inspection of the numerical results immediately reveals that the acoustic modes which are stable for the viscous case when only the κ-mechanism is present, are significantly destabilized when the turbulent diffusion (Cowling) mechanism is included. Likewise, for the non-viscous case the degree of instability of acoustic modes is stronger by a factor of nearly four when the full effects of radiative and turbulent diffusion mechanism are present over the case when only the κ-mechanism operates. We therefore conclude that the five-minute oscillations are driven by a combination of the κ-mechanism and the radiative and turbulent diffusion mechanism the dominant contribution, as measured by the degree of instability, arising from the convective Cowling mechanism.

5. Conclusions

We have investigated the instability of acoustic modes trapped in the solar convection zone by solving the fluid mechanical equations applicable to non-radial, non-adiabatic viscous oscillations in the framework of the linearized theory. The thermodynamic coupling between convection and oscillation is taken into account through the inclusion of the convective flux in the energy equation, while the mechanical effects of turbulence are estimated by introducing an approximate form of turbulent viscosity calculated with the mixing-length approximation. This is admittedly a somewhat simplified prescription for the time-dependent compressible convection. Only a fully non-linear theory can provide a proper framework for this

complex problem, while we have approximated the non-linear effects of the turbulent convection through the eddy diffusivities.

We have treated the turbulent Prandtl number as a free parameter in our work and have attempted to demonstrate that, for the same choice of P_t, it is possible to obtain in a solar envelope model the most unstable convective modes corresponding to granulation and supergranulation and the acoustic modes corresponding to the five-minute oscillations. Considering the uncertainties in the mixing-length formalism, our numerical results are in reasonable accord with the observed scales of motion. It may be noted that the typical scale of supergranulation ($\simeq$30 000 km) is substantially larger than the values given in Table I. These seem to fit better to what has recently been named 'mesogranulation' (cf. November *et al.*, 1981). However, it should be pointed out that the growth rates of C_2-modes are fairly sensitive to various parameters and hence no definite conclusion can be drawn. In this investigation we have neglected the effects of the turbulent pressure; also the viscous dissipation, which is a second-order effect, is absent in the energy equation. This will almost certainly affect the growth rates and the frequencies for large values of the harmonic number l.

We find several acoustic modes trapped in the solar convection zone to be overstable and the most rapidly growing modes occupy a region centred predominantly around a period of 300 s with a wide range of horizontal length scales. The turbulent viscosity has a damping effect on the stability characteristics of the acoustic modes which are sensitively affected by the form of the coefficient of turbulent viscosity.

The essential conclusion of our work is that the turbulent diffusion or convective Cowling mechanism is the physical process that makes a dominant contribution to the generation of self-excited acoustic waves in the solar envelope. This mechanism must be considered in any study of pulsating stars which have convection zones with strongly superadiabatic regions. It is indeed desirable to explore the role of this instability in the context of pulsating stars and especially examine the effect of turbulent viscosity on the red edge of the instability strip.

Appendix

Following Eckart (1960) and Unno *et al.* (1979) we obtain the following equation:

$$\frac{\partial}{\partial t}(\rho E_W)+\nabla\cdot\mathbf{F}_W=\mathbf{v}\nabla\cdot\mathcal{P}-\nabla\cdot\mathbf{F}_1\left[\nabla_{\mathrm{ad}}\frac{P_1}{P_0}+\frac{P_1-c^2\rho_1}{T_0\rho_0 C_{p0}\Gamma_1(\nabla_{\mathrm{ad}}-\nabla)}\right],$$

where

$$E_W=\frac{1}{2}\left[v^2+\left(\frac{P_1}{\rho_0 c}\right)^2+\frac{g^2}{N^2}\left(\frac{P_1}{\Gamma_1 P_0}-\frac{\rho_1}{\rho_0}\right)^2\right];$$

$$\mathbf{F}_W=P_1\mathbf{v}, \qquad \Gamma_1=\left(\frac{\partial \ln P}{\partial \ln \rho}\right)_{\mathrm{ad}};$$

$c^2 = \dfrac{\Gamma_1 P_0}{\rho_0}$ is the square of the sound speed;

$N^2 = -g\left(\dfrac{\mathrm{d} \ln \rho_0}{\mathrm{d}r} - \dfrac{1}{\Gamma_1}\dfrac{\mathrm{d} \ln P_0}{\mathrm{d}r}\right)$ is the square of Brunt-Väisälä frequency;

$\mathscr{P} = \mu(\nabla \mathbf{v} + \mathbf{v}\nabla) - \frac{2}{3}\mu \nabla \cdot \mathbf{v} I$ is the viscous stress tensor,

I being the unit second rank tensor.

Here, E_W and $\mathbf{F}_W$ can be treated as the energy density and the energy flux respectively. Taking the time average over a period of oscillation and integrating over the volume of a sphere of radius r we get

$$\dot{E}_{\mathrm{osc}}(r, t) = \frac{\partial}{\partial t} E_{\mathrm{osc}}(r, t) = \dot{E}_{\mathrm{th}}(r, t) + \dot{E}_{\mathrm{vis}}(r, t) + W_p(r, t) + W_\mu(r, t) .$$

Here

$$E_{\mathrm{osc}}(r, t) = \left\langle \int_V E_W \, \mathrm{d}V \right\rangle ,$$

$$\dot{E}_{\mathrm{th}}(r, t) = \left\langle \int_V -\nabla \cdot \mathbf{F}_1 \left[\nabla_{\mathrm{ad}} \frac{P_1}{P_0} + \frac{P_1 - c^2 \rho_1}{T_0 \rho_0 C_{p0} \Gamma_1 (\nabla_{\mathrm{ad}} - \nabla)} \right] \mathrm{d}V \right\rangle ,$$

$$\dot{E}_{\mathrm{vis}}(r, t) = \left\langle \int_V -\Phi \, \mathrm{d}V \right\rangle ,$$

$$W_p(r, t) = \left\langle \int_S -\mathbf{F}_W \cdot \mathrm{d}\mathbf{S} \right\rangle , \qquad W_\mu(r, t) = \left\langle \int_S \mathscr{P} \cdot \mathbf{v} \, \mathrm{d}\mathbf{S} \right\rangle ,$$

where

$$\Phi = \tfrac{1}{2}\mu_{t0}(\nabla \mathbf{v} + \mathbf{v}\nabla) \cdot (\nabla \mathbf{v} + \mathbf{v}\nabla) - \tfrac{2}{3}\mu_{t0}(\nabla \cdot \mathbf{v})^2$$

is the rate of viscous dissipation per unit volume.

After using the orthogonality and recurrence relations satisfied by the spherical harmonics, we get the following expressions for the various quantities:

$$\mathrm{E}_{\mathrm{osc}}(r, t) = \frac{1}{4} \int_0^r r^2 \, \mathrm{d}r \, \rho_0 \left[|v_r|^2 + l(l+1) |v_h|^2 + \left| \frac{P_1}{\rho_o c} \right|^2 + \frac{g^2}{N^2} \left| \frac{P_1}{\Gamma_1 P_0} - \frac{\rho_1}{\rho_0} \right|^2 \right] ,$$

$$\dot{E}_{\mathrm{th}}(r, t) = \frac{1}{2} \mathrm{Re} \int_0^r r^2 \, \mathrm{d}r (-\nabla \cdot \mathbf{F}_1^*) \left[\nabla_{\mathrm{ad}} \frac{P_1}{P_0} + \frac{P_1 - c^2 \rho_1}{T_0 \rho_0 C_{p0} \Gamma_1 (\nabla_{\mathrm{ad}} - \nabla)} \right] ,$$

$$\dot{E}_{\mathrm{vis}}(r,t) = -\mathrm{Re}\int_0^r \mu_{t0} r^2\,\mathrm{d}r\left[\frac{2}{3}\left|r\frac{\mathrm{d}}{\mathrm{d}r}\left(\frac{v_r}{r}\right)+\frac{l(l+1)}{r}v_h\right|^2+\right.$$

$$+\frac{1}{2}l(l+1)\left|\frac{v_r}{r}+\frac{\mathrm{d}v_h}{\mathrm{d}r}\right|^2-$$

$$\left.-\frac{l(l+1)}{r}\left(\frac{1}{2r}|v_h|^2+\frac{1}{2}\frac{\mathrm{d}}{\mathrm{d}r}|v_h|^2+\frac{v_r^* v_h}{3r}+\frac{2}{3}\frac{\mathrm{d}v_r^*}{\mathrm{d}r}v_h\right)\right],$$

$$W_p(r,t) = -\frac{r^2}{2}\mathrm{Re}\,(P_1^* v_r)\,.$$

References

Ando, H. and Osaki, Y.: 1975, *Publ. Astron. Soc. Japan* **27**, 581.
Antia, H. M.: 1979, *J. Comp. Phys.* **30**, 283.
Antia, H. M., Chitre, S. M., and Kale, D. M.: 1978, *Solar Phys.* **56**, 275.
Antia, H. M., Chitre, S. M., and Pandey, S. K.: 1981, *Solar Phys.* **70**, 67.
Baker, N. H. and Gough, D. O.: 1979, *Astrophys. J.* **234**, 232.
Beckers, J. M. and Canfield, R. C.: 1976, in R. Cayrel and E. P. Steinberg (eds.), *Physique des Mouvements dans les Atmosphères Stellaires*, CNRS No. 250, p. 207.
Berthomieu, G., Cooper, A. J., Gough, D. O., Osaki, Y., Provost, J., and Rocca, A.: 1979, in H. A. Hill and W. A. Dziembowski (eds.), *Proceeding of a Workshop at Tucson*, Arizona, p. 307.
Canfield, R. C.: 1976, *Solar Phys.* **50**, 239.
Cowling, T. G.: 1957, *Magnetohydrodynamics*, New York, Interscience.
Cox, J. P. and Stewart, J. H.: 1970, *Astrophys. J. Suppl.* **19**, 243.
Deubner, F.-L.: 1972, *Solar Phys.* **22**, 263.
Deubner, F.-L.: 1975, *Astron. Astrophys.* **44**, 371.
Deubner, F.-L., Ulrich, R. K., and Rhodes, E. J., Jr.: 1979, *Astron. Astrophys.* **72**, 177.
Eckart, C.: 1960, *Hydrodynamics of Oceans and Atmospheres*, Pergamon Press, London.
Fossat, E., Ricort, G., Aime, C., and Roddier, F.: 1974, *Astrophys. J. Letters* **193**, L97.
Frazier, E. N.: 1968, *Z. Astrophys.* **68**, 345.
Gabriel, M., Scuflaire, R., Noels, A., and Boury, A.: 1975, *Astron. Astrophys.* **40**, 33.
Goldreich, P. and Keeley, D. A.: 1977, *Astrophys. J.* **211**, 934.
Graff, Ph.: 1976, *Astron. Astrophys.* **49**, 299.
Leibacher, J. and Stein, R. F.: 1971, *Astrophys. Letters* **7**, 191.
Leighton, R. B., Noyes, R. W., and Simon, G. W.: 1962, *Astrophys. J.* **135**, 474.
November, L. J., Toomre, J., Gebbie, K. B., and Simon, G. W.: 1981, *Astrophys. J. Letters* **245**, L123.
Rhodes, E. J. Jr., Ulrich, R. K., and Simon, G. W.: 1977, *Astrophys. J.* **218**, 901.
Spiegel, E. A.: 1964, *Astrophys. J.* **139**, 959.
Spruit, H. C.: 1977, Ph.D. Thesis, Utrecht.
Stein, R. F. and Leibacher, J.: 1974, *Ann. Rev. Astron. Astrophys.* **12**, 407.
Tanenbaum, A. S., Wilcox, J. M., Frazier, E. N., and Howard, R.: 1969, *Solar Phys.* **9**, 328.
Ulrich, R. K.: 1970, *Astrophys. J.* **162**, 993.
Ulrich, R. K. and Rhodes, E. J. Jr.: 1977, *Astrophys. J.* **218**, 521.
Unno, W.: 1976, in E. A. Spiegel and J. P. Zahn (eds.), 'Problems of Stellar Convection', *IAU Colloq.* **38**, 315.
Unno, W. and Spiegel, E. A.: 1968, *Publ. Astron. Soc. Japan* **18**, 85.
Unno, W., Osaki, Y., Ando, H., and Shibahashi, H.: 1979, *Nonradial Oscillations of Stars*, University of Tokyo Press, Tokyo.
Vernazza, J. E., Avrett, E. H., and Loeser, R.: 1976, *Astrophys. J. Suppl.* **30**, 1.
Wilkinson, J. H.: 1965, *The Algebraic Eigenvalue Problem*, Oxford Univ. Press, London, New York.